Chapter 3
Digital Holography

3.1 General Principles

The concept of digital holographic recording is illustrated in Fig. 3.1a [196, 198]. A plane reference wave and the wave reflected from the object interfere at the surface of an electronic sensor array (e.g. Charged Coupled Device, CCD, or Complementary Metal Oxide Semiconductor, CMOS). The resulting hologram is electronically recorded and stored in a computer. The object is, in general, a three dimensional body with diffusely reflecting surfaces, located at a distance d from the sensor (measured to some representative plane). This is just the classical off-axis geometry of photographic holography save that the recording medium is an electronic sensor array rather than photographic film.

In classical optical reconstruction using a replica of the original reference wave to illuminate the hologram, a "virtual" (primary) image is recreated at a distance d behind the sensor plane as viewed by an observer; a "real" (secondary) image is also formed at a distance d, from the sensor but in front of it, between it and the observer, see Fig. 3.1b. In DH, though, a physical image in virtual or real space is not created; numerical reconstruction by computer at a given plane produces a primary or secondary image on a monitor.

Using the coordinate system of Fig. 3.2, a light wave diffracted at an aperture (in this case a hologram) perpendicular to an incoming beam is described by the Fresnel-Kirchhoff integral, see Eq. (2.48), as

$$\Gamma(\xi', \eta') = \frac{i}{\lambda} \int_{-\infty}^{\infty} \int_{-\infty}^{\infty} h(x,y) E_R(x,y) \frac{\exp\left(-i\frac{2\pi}{\lambda}\rho'\right)}{\rho'} dxdy \qquad (3.1)$$

U. Schnars et al., *Digital Holography and Wavefront Sensing*,
DOI 10.1007/978-3-662-44693-5_3

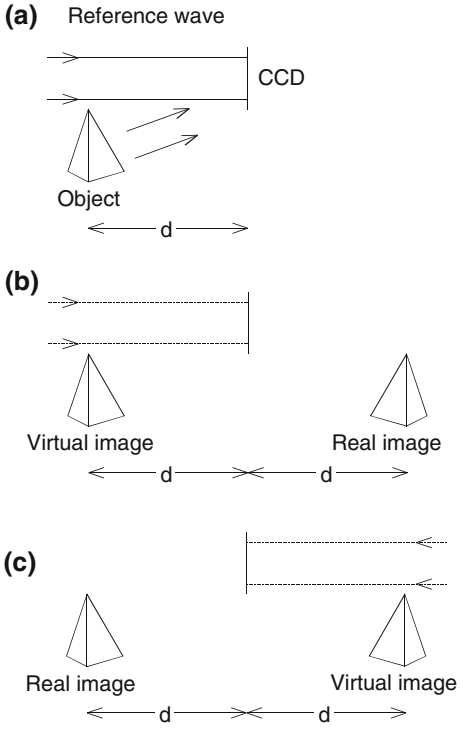

Fig. 3.1 Digital Holography. **a** Recording, **b** Reconstruction with reference wave $E_{R,}$ **c** Reconstruction with conjugate reference wave E_R^*

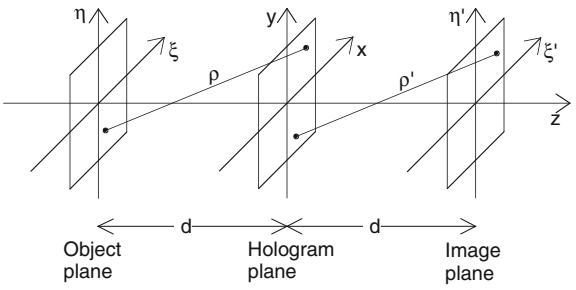

Fig. 3.2 Coordinate system for numerical hologram reconstruction

where

$$\rho' = \sqrt{(x-\xi')^2+(y-\eta')^2+d^2} \tag{3.2}$$

h(x,y) is the hologram function and ρ' is the distance between a point in the hologram plane and a point in the reconstruction plane. The inclination factor is set to 1, since the angles θ' and θ'' (see Sect. 2.4) are approximately zero. This is valid for all the numerical reconstruction algorithms in this book.

A plane reference wave $E_R(x,y)$ can be described in terms of its real amplitude,

$$E_R = a_R + i0 = a_R \tag{3.3}$$

The diffraction pattern is calculated at a distance d behind the sensor plane, so that it reconstructs the complex amplitude of the wave in the plane of the real image.

Equation (3.1) forms the basis for numerical reconstruction from a hologram. Because the reconstructed wave field $\Gamma(\xi',\eta')$ is a complex function, both the intensity as well as its phase can be extracted [195]. This is in contrast to the case of optical hologram reconstruction, in which only the intensity is obtainable. This interesting property of Digital Holography is used in Digital Holographic Interferometry, see Chap. 4.

As discussed in Sect. 2.6 the real image could be distorted. According to Eq. (2.63) an undistorted real image can be produced by using the conjugate reference beam for reconstruction. To numerically reconstruct an undistorted real image it is therefore necessary to insert E_R^* instead of E_R into Eq. (3.1):

$$\Gamma(\xi,\eta) = \frac{i}{\lambda}\int_{-\infty}^{\infty}\int_{-\infty}^{\infty} h(x,y)E_R^*(x,y)\frac{\exp\left(-i\frac{2\pi}{\lambda}\rho\right)}{\rho}dxdy \tag{3.4}$$

with

$$\rho = \sqrt{(x-\xi)^2+(y-\eta)^2+d^2} \tag{3.5}$$

This reconstruction scheme is shown in Fig. 3.1c. The real image is formed at the position where the object was located during recording. It should be noted that for the plane reference wave defined in Eq. (3.3) both reconstruction formulas, Eqs. (3.1) and (3.4), are equivalent since $E_R = E_R^* \equiv a_R$.

The arrangement of Fig. 3.1 with a plane reference wave perpendicularly illuminating the sensor is commonly used in Digital Holography. Other recording geometries are discussed later.

Reconstruction of the virtual image is also possible by either selecting the negative branch of the square root or introducing the imaging properties of a lens into the numerical reconstruction process [196]. This lens corresponds to the eye of an observer viewing an optically reconstructed hologram. In the simplest case this lens is located directly behind the hologram, as in Fig. 3.3. The imaging properties of a lens with focal distance f are represented by a complex factor, $L(x,y)$, as

$$L(x,y) = \exp\left[i\frac{\pi}{\lambda f}\left(x^2+y^2\right)\right] \tag{3.6}$$

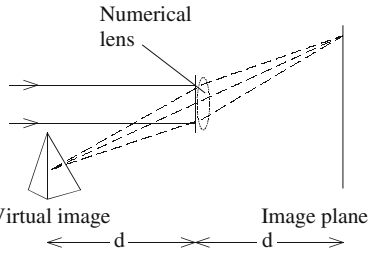

Fig. 3.3 Reconstruction of the virtual image

The factor L(x,y) is calculated in Annex B1. For unity magnification, the lens should have a focal length of $f = d/2$.

The lens described by Eq. (3.6) introduces phase aberrations, which can be corrected by multiplying the reconstructed wave field by another factor

$$P(\xi', \eta') = \exp\left[i\frac{\pi}{\lambda f}\left(\xi'^2 + \eta'^2\right)\right] \tag{3.7}$$

This correction factor is derived in Annex B2. The full equation which describes reconstruction via a virtual lens with $f = d/2$ is therefore

$$\Gamma(\xi', \eta') = \frac{i}{\lambda}P(\xi', \eta')\int_{-\infty}^{\infty}\int_{-\infty}^{\infty} h(x,y)E_R(x,y)L(x,y)\frac{\exp\left(-i\frac{2\pi}{\lambda}\rho'\right)}{\rho'}dxdy \tag{3.8}$$

3.2 Numerical Reconstruction

3.2.1 Reconstruction by the Fresnel Approximation

For x- and y-values, as well as for ξ- and η-values, which are small compared to the distance d between the reconstruction plane and the sensor, the expression Eq. (3.5) can be expanded with a Taylor series:

$$\rho = d + \frac{(\xi - x)^2}{2d} + \frac{(\eta - y)^2}{2d} - \frac{1}{8}\frac{\left[(\xi - x)^2 + (\eta - y)^2\right]^2}{d^3} + \cdots \tag{3.9}$$

The fourth term in Eq. (3.9) can be neglected, if it is small compared to the wavelength [116], i.e. if,

$$\frac{1}{8}\frac{\left[(\xi - x)^2 + (\eta - y)^2\right]^2}{d^3} \ll \lambda \tag{3.10}$$

Or, rewriting in terms of d, we have

$$d \gg \sqrt[3]{\frac{1}{8}\frac{[(\xi - x)^2 + (\eta - y)^2]^2}{\lambda}} \tag{3.11}$$

Then the distance ρ consists of linear and quadratic terms:

$$\rho = d + \frac{(\xi - x)^2}{2d} + \frac{(\eta - y)^2}{2d} \tag{3.12}$$

With the additional approximation of replacing the denominator in (3.4) by d the following expression results for reconstruction of the real image:

$$\Gamma(\xi, \eta) = \frac{i}{\lambda d}\exp\left(-i\frac{2\pi}{\lambda}d\right) \times \int_{-\infty}^{\infty}\int_{-\infty}^{\infty} E_R^*(x, y)h(x, y)\exp\left[-i\frac{\pi}{\lambda d}\left((\xi - x)^2 + (\eta - y)^2\right)\right]dxdy \tag{3.13}$$

If the multiplication terms in the argument of the exponential under the integral are carried out we get

$$\Gamma(\xi, \eta) = \frac{i}{\lambda d}\exp\left(-i\frac{2\pi}{\lambda}d\right)\exp\left[-i\frac{\pi}{\lambda d}\left(\xi^2 + \eta^2\right)\right] \times \int_{-\infty}^{\infty}\int_{-\infty}^{\infty} E_R^*(x, y)h(x, y)\exp\left[-i\frac{\pi}{\lambda d}\left(x^2 + y^2\right)\right]\exp\left[i\frac{2\pi}{\lambda d}(x\xi + y\eta)\right]dxdy \tag{3.14}$$

This equation is known as the *Fresnel approximation* or *Fresnel transformation* due to its mathematical similarity with the Fourier Transform (see below). It enables reconstruction of the wavefield in a plane behind the hologram, in this case in the plane of the real image.

The intensity is given by its square,

$$I(\xi, \eta) = |\Gamma(\xi, \eta)|^2 \tag{3.15}$$

and its phase by

$$\varphi(\xi, \eta) = \arctan\frac{\mathrm{Im}[\Gamma(\xi, \eta)]}{\mathrm{Re}[\Gamma(\xi, \eta)]} \tag{3.16}$$

where "Re" denotes the real part and "Im" the imaginary part of the wave.

Reconstruction of the virtual image in the Fresnel approximation can be expressed as,

$$\begin{aligned}\Gamma(\xi',\eta') &= \frac{i}{\lambda d}\exp\left(-i\frac{2\pi}{\lambda}d\right)\exp\left[-i\frac{\pi}{\lambda d}\left(\xi'^2+\eta'^2\right)\right]P(\xi',\eta')\\ &\quad\times\int_{-\infty}^{\infty}\int_{-\infty}^{\infty}E_R(x,y)L(x,y)h(x,y)\exp\left[-i\frac{\pi}{\lambda d}\left(x^2+y^2\right)\right]\exp\left[i\frac{2\pi}{\lambda d}\left(x\xi'+y\eta'\right)\right]dxdy\\ &= \frac{i}{\lambda d}\exp\left(-i\frac{2\pi}{\lambda}d\right)\exp\left[+i\frac{\pi}{\lambda d}\left(\xi'^2+\eta'^2\right)\right]\\ &\quad\times\int_{-\infty}^{\infty}\int_{-\infty}^{\infty}E_R(x,y)h(x,y)\exp\left[+i\frac{\pi}{\lambda d}\left(x^2+y^2\right)\right]\exp\left[i\frac{2\pi}{\lambda d}\left(x\xi'+y\eta'\right)\right]dxdy\end{aligned} \tag{3.17}$$

Alternatively we can insert a negative distance into Eq. (3.14), which has the added advantage that the virtual image is not rotated by 180° because of the action of performing the Fourier transform.

To digitise the Fresnel transform in Eq. (3.14), the following definitions and substitutions are introduced [261],

$$u=\frac{\xi}{\lambda d};\quad v=\frac{\eta}{\lambda d} \tag{3.18}$$

Thus (3.14) is now expressed as,

$$\begin{aligned}\Gamma(u,v) &= \frac{i}{\lambda d}\exp\left(-i\frac{2\pi}{\lambda}d\right)\exp\left[-i\pi\lambda d\left(u^2+v^2\right)\right]\\ &\quad\times\int_{-\infty}^{\infty}\int_{-\infty}^{\infty}E_R^*(x,y)h(x,y)\exp\left[-i\frac{\pi}{\lambda d}\left(x^2+y^2\right)\right]\exp[i2\pi(xu+yv)]dxdy\end{aligned} \tag{3.19}$$

A comparison of Eq. (3.19) with the definition of the two-dimensional Fourier transform (see Annex A) shows that the Fresnel approximation is the just the inverse Fourier transformation of the function $E_R^*(x,y)h(x,y)\exp[-i\pi/\lambda d(x^2+y^2)]$,

$$\begin{aligned}\Gamma(u,v) &= \frac{i}{\lambda d}\exp\left(-i\frac{2\pi}{\lambda}d\right)\exp\left[-i\pi\lambda d\left(u^2+v^2\right)\right]\\ &\quad\times\Im^{-1}\left\{E_R^*(x,y)h(x,y)\exp\left[-i\frac{\pi}{\lambda d}\left(x^2+y^2\right)\right]\right\}\end{aligned} \tag{3.20}$$

The function Γ can be digitised if the hologram function $h(x,y)$ is sampled on a rectangular raster of N × N points, with steps Δx and Δy along the coordinates. The

distances between neighbouring pixels on the sensor array in the horizontal and vertical directions are given by Δx and Δy respectively. With these discrete values included, the integrals in (3.19) are written in terms of finite sums, i.e.

$$\Gamma(m,n) = \frac{i}{\lambda d}\exp\left(-i\frac{2\pi}{\lambda}d\right)\exp\left[-i\pi\lambda d\left(m^2\Delta u^2 + n^2\Delta v^2\right)\right] \times \sum_{k=0}^{N-1}\sum_{l=0}^{N-1} E_R^*(k,l)h(k,l)\exp\left[-i\frac{\pi}{\lambda d}\left(k^2\Delta x^2 + l^2\Delta y^2\right)\right]\exp[i2\pi(k\Delta x m\Delta u + l\Delta y n\Delta v)]$$

$$\text{for } m = 0, 1, ..., N-1; \text{and } n = 0, 1, \ldots, N-1 \tag{3.21}$$

According to Fourier transform procedures, and Δu, Δv can be written in terms of Δx, Δy (see Annex A) as,

$$\Delta u = \frac{1}{N\Delta x}; \quad \Delta v = \frac{1}{N\Delta y} \tag{3.22}$$

After re-substitution, we have,

$$\Delta\xi = \frac{\lambda d}{N\Delta x}; \quad \Delta\eta = \frac{\lambda d}{N\Delta y} \tag{3.23}$$

Applying these relationships, Eq. (3.21) converts to

$$\Gamma(m,n) = \frac{i}{\lambda d}\exp\left(-i\frac{2\pi}{\lambda}d\right)\exp\left[-i\pi\lambda d\left(\frac{m^2}{N^2\Delta x^2} + \frac{n^2}{N^2\Delta y^2}\right)\right] \times \sum_{k=0}^{N-1}\sum_{l=0}^{N-1} E_R^*(k,l)h(k,l)\exp\left[-i\frac{\pi}{\lambda d}\left(k^2\Delta x^2 + l^2\Delta y^2\right)\right]\exp\left[i2\pi\left(\frac{km}{N} + \frac{ln}{N}\right)\right] \tag{3.24}$$

This is the discrete Fresnel transform. The matrix Γ is evaluated by multiplying $E_R^*(k,l)$ with $h(k,l)$ and $\exp[-i\pi/(\lambda d)(k^2\Delta x^2 + l^2\Delta y^2)]$, followed by application of an inverse discrete Fourier transform to the product. This calculation is accomplished most efficiently using the Fast Fourier Transform (FFT) algorithm. The factors before the sum term in Eq. (3.24) only affect the overall phase and can be neglected if it is only the intensity in Eq. (3.15) that is of interest. This is also the case if phase differences between holograms recorded with the same wavelength have to be calculated, according to,$(\Delta\varphi = \varphi_1 + const. - (\varphi_2 + const.) = \varphi_1 - \varphi_2)$.

The corresponding discrete formula for reconstruction with a virtual lens of $f = d/2$ (Eq. 3.17) is,

$$\Gamma(m,n) = \frac{i}{\lambda d}\exp\left(-i\frac{2\pi}{\lambda}d\right)\exp\left[+i\pi\lambda d\left(\frac{m^2}{N^2\Delta x^2}+\frac{n^2}{N^2\Delta y^2}\right)\right] \times \sum_{k=0}^{N-1}\sum_{l=0}^{N-1} E_R(k,l)h(k,l)\exp\left[+i\frac{\pi}{\lambda d}\left(k^2\Delta x^2+l^2\Delta y^2\right)\right]\exp\left[i2\pi\left(\frac{km}{N}+\frac{ln}{N}\right)\right] \tag{3.25}$$

A typical digital hologram of a dice recorded with the geometry of Fig. 3.1 is shown in Fig. 3.4. The dice is placed a distance d = 1.054 m from a sensor array with 1,024 × 1,024 pixels of pitch $\Delta x = \Delta y = 6.8$ μm. The recording wavelength is 632.8 nm. Numerical reconstruction of the real image is performed according to Eqs. (3.14) and (3.24) and illustrated in Fig. 3.5. The bright square in the centre of the image is the non-diffracted (zero order) reconstruction wave and corresponds to the first term on the right side of Eq. (2.63). Because of the off-axis geometry, the image is spatially separated from the zero order term. The other (virtual) image is out-of-focus in this reconstruction.

An interesting property of (off-axis) holography is that every part of a hologram contains all the information about the entire object. This is illustrated by the holograms of Figs. 3.6 and 3.8, where black masks cover nearly half of the hologram areas. Nevertheless, the entire cube is visible without obstruction in the reconstructions (Figs. 3.7 and 3.9). The masks are visible as shadows in the zero order terms. The reduction of the effective pixel number leads to a consequent

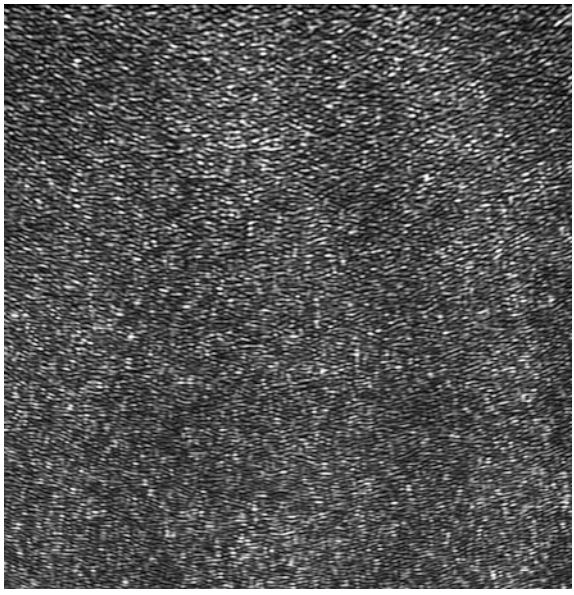

Fig. 3.4 Digital hologram of a die

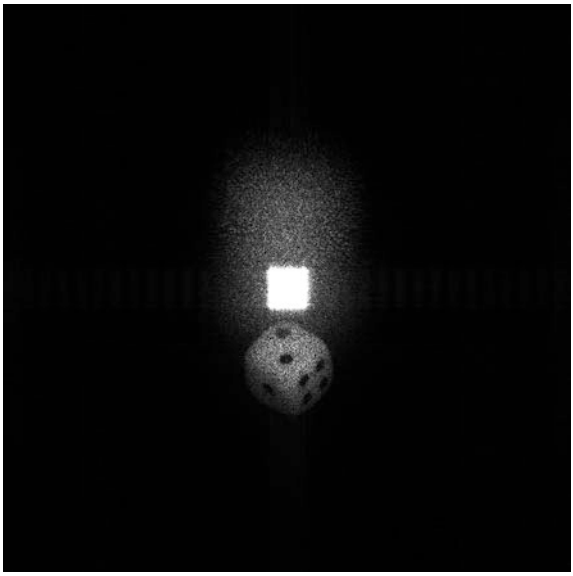

Fig. 3.5 Numerical reconstruction

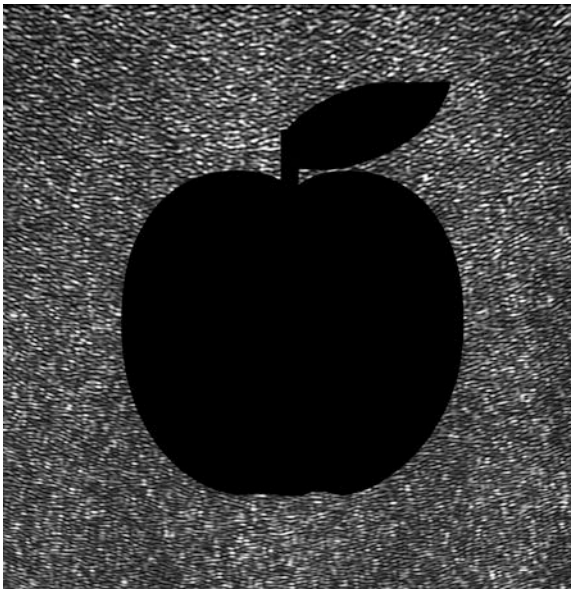

Fig. 3.6 Masked digital hologram

reduction of the resolution in the reconstructed images. This is equivalent to the increase of the speckle size observed in optical hologram reconstruction when the aperture is reduced.

Regarding Eq. (3.23), the pixel distances in the reconstructed image $\Delta\xi$ and $\Delta\eta$ are dependent on the chosen numerical reconstruction distance d. This is because

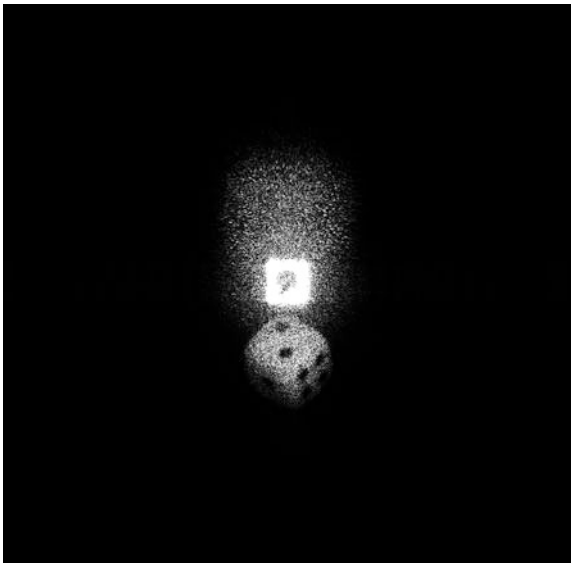

Fig. 3.7 Reconstruction

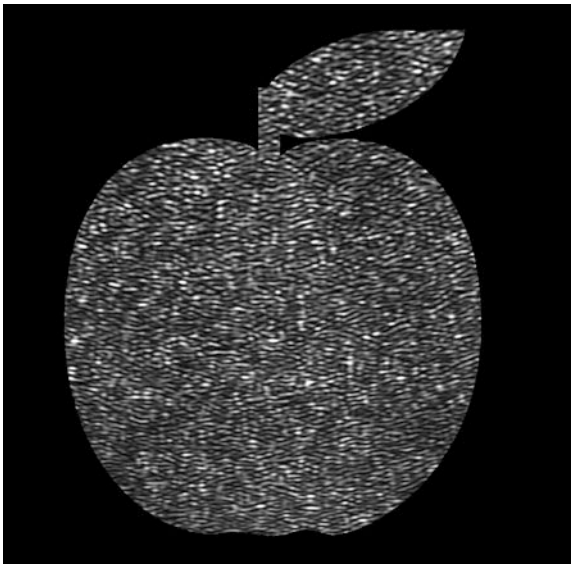

Fig. 3.8 Masked digital hologram

Eq. (3.23) corresponds to the diffraction limited resolution of an optical system. The hologram corresponds to the aperture of the optical system with a side of length $N\Delta x$; a diffraction pattern develops at a distance d behind the hologram. The term $\Delta\xi = \lambda d/N\Delta x$ therefore describes the half-diameter of the Airy disk or the speckle diameter in the plane of the reconstructed image, accordingly, limits the resolution.

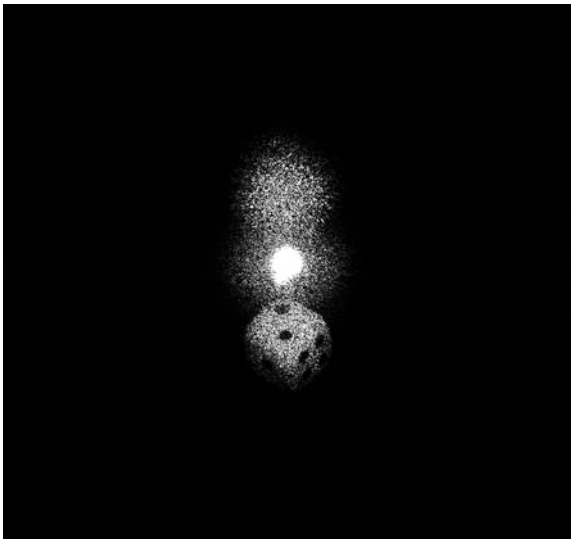

Fig. 3.9 Reconstruction

This can be regarded as a "natural scaling" algorithm, setting the resolution of the image reconstructed by a discrete Fresnel transform always to the physical limit.

A simple Matlab© Fresnel transformation reconstruction routine is shown in Appendix C.

3.2.2 Reconstruction by the Convolution Approach

Numerical processing of the Fresnel-Kirchhoff integral Eqs. (3.1) and (3.4) without the application of any approximations is time consuming. For faster and more efficient numerical processing, a different but equivalent formulation is often more suitable. This formulation makes use of the convolution theorem and, within the scope of this book, is accordingly denoted as the "convolution approach". Some other publications use the term *Angular Spectrum Method* (ASM), see e.g. [243]. Demetrakopoulos and Mittra applied this method for numerical reconstruction of suboptical holograms [41]. Later this approach was applied to optical holography by Kreis [124].

The reconstruction formula Eq. (3.4) can be interpreted as a superposition integral,

$$\Gamma(\xi,\eta) = \int_{-\infty}^{\infty}\int_{-\infty}^{\infty} h(x,y)E_R^*(x,y)g(\xi,\eta,x,y)dxdy \tag{3.26}$$

where the impulse response $g(x,y,\xi,\eta)$ is given by

$$g(\xi,\eta,x,y) = \frac{i}{\lambda}\frac{\exp\left[-i\frac{2\pi}{\lambda}\sqrt{d^2+(x-\xi)^2+(y-\eta)^2}\right]}{\sqrt{d^2+(x-\xi)^2+(y-\eta)^2}} \tag{3.27}$$

According to Eq. (3.26) the linear system characterized by $g(\xi,\eta,x,y) = g(\xi-x,\eta-y)$ is shift-invariant. The superposition integral can be regarded therefore as a convolution and the convolution theorem (Annex A) can be applied. According to this approach the Fourier transform of the convolution of $h \cdot E_R^*$ with g is the product of the individual transforms $\Im\{hE_R^*\}$ and $\Im\{g\}$. So $\Gamma(\xi,\eta)$ can be calculated by, firstly Fourier transforming $h \cdot E_R^*$, followed by multiplication with the Fourier transform of g, and, finally, taking an inverse Fourier transform of the product. Three Fourier transforms are therefore necessary to complete the whole process. The individual Fourier transforms are efficiently carried out using the FFT algorithm.

For numerical processing the discrete impulse response function has to be calculated, by replacing the continuous differences $(x-\xi)$ and $(y-\eta)$ with the discrete variables $k\Delta x$ and $l\Delta y$, thus

$$g(k,l) = \frac{i}{\lambda}\frac{\exp\left[-i\frac{2\pi}{\lambda}\sqrt{d^2+k^2\Delta x^2+l^2\Delta y^2}\right]}{\sqrt{d^2+k^2\Delta x^2+l^2\Delta y^2}} \tag{3.28}$$

with integer values $k = 0,1,\ldots,N-1$; $l = 0,1,\ldots,N-1$

The process of reconstruction into the real image plane can be written as,

$$\Gamma(\xi,\eta) = \Im^{-1}\left\{\Im\left(h \cdot E_R^*\right) \cdot \Im(g)\right\} \tag{3.29}$$

A simple Matlab© reconstruction routine perform Eq. (3.29) is shown in Appendix C.

The Fourier transform of $g(\xi,\eta,x,y)$ can be calculated and expressed analytically [130] as,

$$G\left(f_x,f_y\right) = \exp\left(-i\frac{2\pi d}{\lambda}\sqrt{1-\lambda^2 f_x^2-\lambda^2 f_y^2}\right) \tag{3.30}$$

The spatial frequencies f_x and f_y can now be replaced by discrete values,

$$f_x = \frac{n}{N\Delta x} \quad f_y = \frac{m}{N\Delta y} \tag{3.31}$$

with integer values $n = 0,1,\ldots,N-1$; $m = 0,1,\ldots,N-1$. The discrete transfer function G now becomes

$$G(n,m) = \exp\left\{-i\frac{2\pi d}{\lambda}\sqrt{1-\left(\frac{\lambda n}{N\Delta x}\right)^2-\left(\frac{\lambda m}{N\Delta y}\right)^2}\right\} \tag{3.32}$$

which consequently saves one Fourier transform operation in reconstruction. Thus we now have,

$$\Gamma(\xi,\eta) = \Im^{-1}\left\{\Im\left(h\cdot E_R^*\right)\cdot G\right\} \tag{3.33}$$

To reconstruct the virtual image either a negative distance, or a lens with transmission factor $L(x,y)$ and a correction factor $P(\xi',\eta')$ according to Eqs. (3.6) and (3.7) have to be taken into account. Thus, we have

$$\Gamma(\xi',\eta') = P(\xi',\eta')\Im^{-1}\{\Im(h\cdot E_R\cdot L)\cdot G\} \tag{3.34}$$

The pixel spacing corresponding to the images reconstructed by the convolution approach are equal to that of the hologram pitch, i.e.

$$\Delta\xi = \Delta x; \quad \Delta\eta = \Delta y \tag{3.35}$$

The pixel separations in the reconstructed images corresponding to the convolution approach differ from those which occur with the Fresnel approximation (Eq. 3.23). At first sight it seems to be possible to achieve a higher resolution with the convolution approach if the pixel separation is small enough. However, on closer examination we recognise that the resolution calculated by Eq. (3.35) is only a numerical value. The physical image resolution is determined by the diffraction limit, i.e. Eq. (3.23) and this also applies to the resolution limit corresponding to the convolution approach.

The area reconstructed with the impulse response function defined in Eq. (3.32) is symmetrical with respect to the optical axis. The area can be shifted by introducing the integers s_k, l_l,

$$g(k+s_k,l+s_l) = \frac{i}{\lambda}\frac{\exp\left[-i\frac{2\pi}{\lambda}\sqrt{d^2+(k+s_k)^2\Delta x^2+(l+s_l)^2\Delta y^2}\right]}{\sqrt{d^2+(k+s_k)^2\Delta x^2+(l+s_l)^2\Delta y^2}} \tag{3.36}$$

The convolution approach allows us to introduce image magnification into the reconstruction process. This is possible if the reconstruction distance is set to

$$d' = d\cdot m \tag{3.37}$$

where d is the recording distance (also used as the reconstruction distance) and m is the magnification factor. A magnification of $m = 1$ corresponds to $\Delta\xi = \Delta x$, and $\Delta\eta = \Delta y$. The lens focal distance is given by the lens formula of geometrical optics:

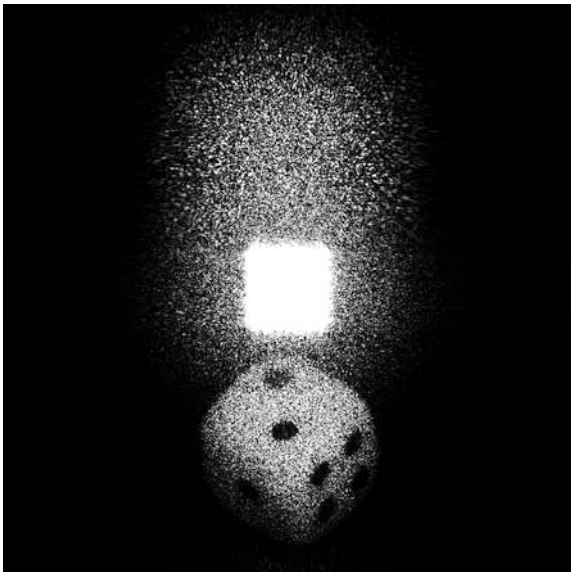

Fig. 3.10 Reconstruction with the convolution approach

$$f = \left(\frac{1}{d} + \frac{1}{d'}\right)^{-1} \tag{3.38}$$

Now Eq. (3.34) is applied for reconstruction at a distance d' instead of d and, thus

$$L(x,y) = \exp\left[i\frac{\pi}{\lambda f}\left(x^2 + y^2\right)\right] = \exp\left[i\frac{\pi}{\lambda}\left(\frac{1}{d} + \frac{1}{d'}\right)\left(x^2 + y^2\right)\right] \tag{3.39}$$

An example of a reconstruction with the convolution approach is shown in Fig. 3.10. The hologram of Fig. 3.4 is reconstructed with a magnification of $m = 1/7$. The corresponding pixel separation in the reconstructed image for Δx of 6.8 μm is given as $\Delta\xi = \Delta x/m = 48\ \mu$m. This should be compared with $\Delta\xi =$ 96 μm obtained using the Fresnel reconstruction (and shown in Fig. 3.5). Thus twice as many pixels are available for the object field using the convolution approach. However, it is emphasized again that the physical resolution is the same in both Figs. 3.5 and 3.10.

3.2.3 Digital Fourier Holography

The special holographic recording geometry of Fig. 3.11 is known as *lensless Fourier holography*. It also has been realized using digital holographic concepts

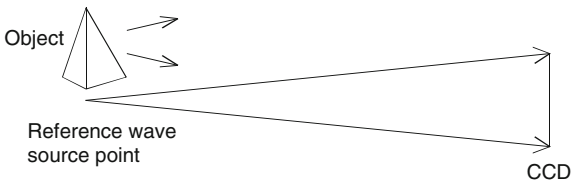

Fig. 3.11 Digital lensless Fourier holography

[245]. Here, a point source spherical reference wave is located in the plane of the object. The reference wave at the sensor plane is therefore described by,

$$E_R = \frac{\exp\left(-i\frac{2\pi}{\lambda}\sqrt{(d^2+x^2+y^2)}\right)}{\sqrt{(d^2+x^2+y^2)}} \approx \frac{1}{d}\exp\left(-i\frac{2\pi}{\lambda}d\right)\exp\left(-i\frac{\pi}{\lambda d}\left(x^2+y^2\right)\right) \tag{3.40}$$

The term $\sqrt{d^2+x^2+y^2}$ is the distance between the point source and a point with coordinates *(x,y)* in the sensor plane. The approximation in Eq. (3.40) is the same as used in Sect. 3.2.1 to derive the Fresnel transform. Inserting this expression into the reconstruction formula for the virtual image (3.17) leads to following equation,

$$\Gamma(\xi,\eta) = C\exp\left[+i\frac{\pi}{\lambda d}\left(\xi^2+\eta^2\right)\right]\Im^{-1}\{h(x,y)\} \tag{3.41}$$

where C is a complex constant. A lensless Fourier hologram is therefore reconstructed by a Fourier transform. The spherical phase factor $\exp(-i\pi/\lambda d(x^2+y^2))$ associated with the Fresnel transform is eliminated by the use of a spherical reference wave with the same curvature as the original. Numerical focusing into other planes is therefore not possible using Eq. (3.41). Numerical focusing can be realized, if different values of d for *recording* (reference wave factor E_R) and *reconstruction* are inserted in Eq. (3.17).

3.3 Shift and Suppression of DC-Term and Conjugate Image

3.3.1 Suppression of the DC Term

The bright square in the centre of Fig. 3.5 is the non-diffracted reconstruction wave. This zero order or DC term disturbs the image, because it obscures all the parts of the object which lie behind it. Methods have been developed to suppress this term e. g. by Kreis et al. [125].

To understand the origins of this DC term, the process of hologram formation as described by Eq. (2.60) needs to be considered again. The equation is rewritten by inserting the definitions of E_R and E_O, and multiplying, to give,

$$\begin{aligned} I(x,y) &= |E_0(x,y) + E_R(x,y)|^2 \\ &= a_R^2 + a_O^2 + 2a_R a_O \cos(\varphi_O - \varphi_R) \end{aligned} \tag{3.42}$$

The first two terms lead to the DC term in the reconstruction process. The third term is a cosinusoidally varying component lying between values of $\pm 2a_R a_O$ and illuminating the pixels across the sensor. The average intensity of all pixels of the hologram matrix is

$$I_m = \frac{1}{N^2} \sum_{k=0}^{N-1} \sum_{l=0}^{N-1} I(k\Delta x, l\Delta y) \tag{3.43}$$

The term $a_R^2 + a_O^2$ can now be suppressed by subtracting this average intensity I_m from the hologram:

$$I'(k\Delta x, l\Delta y) = I(k\Delta x, l\Delta y) - I_m(k\Delta x, l\Delta y) \tag{3.44}$$

for $k = 0, \ldots, N-1; \quad l = 0, \ldots, N-1$.

The reconstruction of I' creates an image with strongly suppressed DC term. An example of this is shown in Fig. 3.12. The upper left figure is a photograph of the object. Reconstruction without DC term suppression is depicted in the upper right figure. The object is covered by the DC term. The lower left figure shows reconstruction with DC suppression included. The original object is clearly visible.

Instead of subtracting the average intensity it is also possible remove the DC component using a high-pass filter with a low cut-off frequency as shown in the lower right image of Fig. 3.12.

The subtraction of the average intensity from the hologram before reconstruction is the basic objective of DC suppression. The same effect can be achieved, if two holograms with stochastically changed speckle structures are subtracted from each other [42]. The reconstruction of this subtraction hologram results in an image without zero order term.

Another method of suppression is to separately capture and measure the intensities of the reference wave a_R^2 and object wave a_O^2. This can be done for example by blocking one wave while monitoring the other. Afterwards a DC term free image can be calculated by subtracting the intensities from the hologram before reconstruction. However, this requires higher experimental effort due to the additional measurements needed.

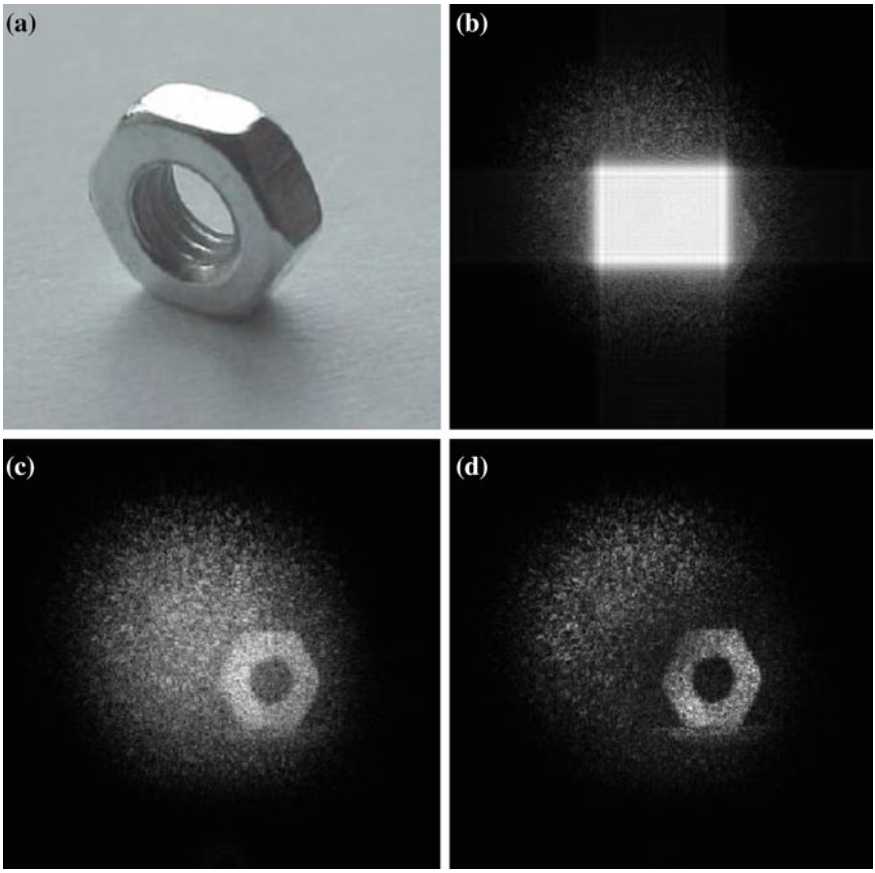

Fig. 3.12 Suppression of the DC term (courtesy of S. Seebacher)

3.3.2 Tilted Reference Wave

Using the recording geometry of Fig. 3.1 the real and virtual image are located at different observation planes. During numerical reconstruction we can choose to focus either on the real or on the virtual image. The other image is usually out-of-focus due to the long distance between the object and sensor. Consequently only one image is clearly visible in the reconstruction, see Fig. 3.5.

However, there are some instances where it is beneficial to laterally shift one image with respect to the other. In this case it can be useful to record the holograms with a tilted reference wave, as in Fig. 3.13. In this geometry the real image is deflected from the optic axis at an angle approximately twice that of the original reference wave.

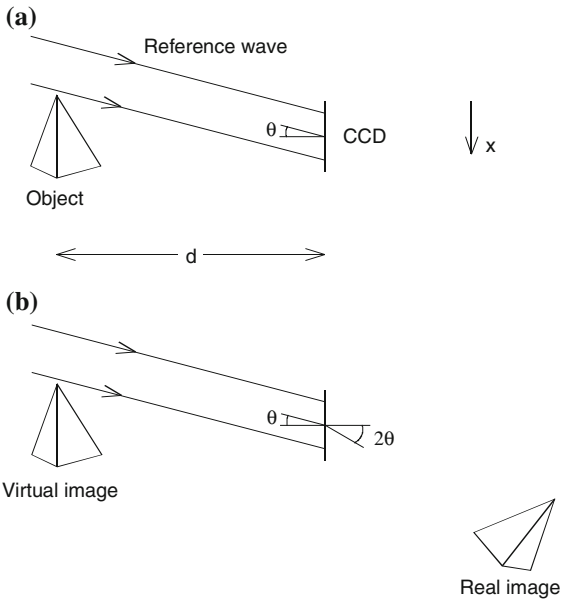

Fig. 3.13 Digital Holography with a tilted reference wave. **a** Recording. **b** Reconstruction

The tilted reference wave is described by,

$$E_R = \exp\left(-i\frac{2\pi}{\lambda}x\sin\theta\right) \tag{3.45}$$

The disadvantage of this set-up are the much higher spatial frequencies produced at the sensor in comparison to the geometry of Fig. 3.1.

3.3.3 Phase Shifting Digital Holography

The amplitude and phase of a light wave can be reconstructed from a single hologram by the methods described in the preceding chapters. A completely different approach, called Phase Shifting Digital Holography, has been proposed by Skarman [216, 251]. He used a phase shifting algorithm to calculate the *initial* phase and thus the complex amplitude in any plane, e.g. the image plane. With the initial complex amplitude distribution in one plane the wave field in any other plane can be determined using the Fresnel-Kirchhoff formulation. Later Phase Shifting DH was improved and applied to opaque objects by Yamaguchi et al. [92, 255–258, 264, 265].

The basic arrangement for phase shifting DH is shown in Fig. 3.14. The object wave and the reference wave interfere at the surface of a sensor. The reference wave is guided via a mirror mounted on a piezoelectric transducer (PZT). With this PZT

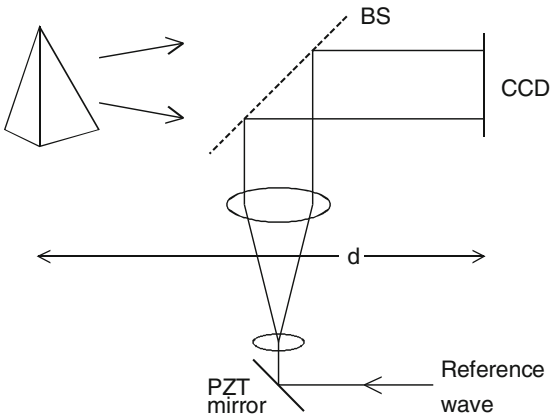

Fig. 3.14 Phase shifting Digital Holography, set-up

the phase of the reference wave can be shifted stepwise. Several (at least three) interferograms with mutual phase shifts are recorded. Afterwards the object phase φ_O is calculated from the phase shifted interferograms; the procedure is similar to that of phase shifting in conventional HI (see Sect. 2.7.5). The real amplitude $a_O(x,y)$ of the object wave can be extracted from the intensity by blocking the reference wave.

As a result the complex amplitude

$$E_O(x,y) = a_O(x,y)\exp(+i\varphi_O(x,y)) \tag{3.46}$$

of the object wave is determined in the recording (x,y) plane.

Now the Fresnel-Kirchhoff integral can be used to calculate the complex amplitude in any other plane. To calculate an image of the object an artificial lens with, for example, $f = d/2$ is introduced in the recording plane according to Eq. (3.6). By means of the Fresnel approximation Eq. (3.17) the complex amplitude in the image plane is then given by

$$\begin{aligned} E_O(\xi',\eta') &= C\exp\left[+i\frac{\pi}{\lambda d}\left(\xi'^2+\eta'^2\right)\right] \\ &\quad\times\int_{-\infty}^{\infty}\int_{-\infty}^{\infty} E_O(x,y)L(x,y)\exp\left[-i\frac{\pi}{\lambda d}\left(x^2+y^2\right)\right]\exp\left[i\frac{2\pi}{\lambda d}(x\xi'+y\eta')\right]dxdy \\ &= C\exp\left[+\frac{i\pi}{\lambda d}\left(\xi'^2+\eta'^2\right)\right] \\ &\quad\times\int_{-\infty}^{\infty}\int_{-\infty}^{\infty} E_O(x,y)\exp\left[+i\frac{\pi}{\lambda d}\left(x^2+y^2\right)\right]\exp\left[i\frac{2\pi}{\lambda d}(x\xi'+y\eta')\right]dxdy \end{aligned} \tag{3.47}$$

where again the coordinate system of Fig. 3.2 applies. Since the complex amplitude in the hologram plane is known, it is also possible to reconstruct the object by inversion of the propagation process [206]. Propagation from the object plane to the hologram plane is described by

$$E_O(x,y) = \frac{i}{\lambda}\int_{-\infty}^{\infty}\int_{-\infty}^{\infty} E_O(\xi,\eta)\frac{\exp\left(-i\frac{2\pi}{\lambda}\sqrt{d^2+(\xi-x)^2+(\eta-y)^2}\right)}{\sqrt{d^2+(\xi-x)^2+(\eta-y)^2}}d\xi d\eta \\ = \Im^{-1}\{\Im(E_O(\xi,\eta))\cdot\Im(g(\xi,\eta,x,y))\} \tag{3.48}$$

with

$$g(\xi,\eta,x,y) = \frac{i}{\lambda}\frac{\exp\left(-i\frac{2\pi}{\lambda}\sqrt{d^2+(\xi-x)^2+(\eta-y)^2}\right)}{\sqrt{d^2+(\xi-x)^2+(\eta-y)^2}} \tag{3.49}$$

$E_O(\xi,\eta)$ describes the complex amplitude of the object wave at the surface, see Fig. 3.2. Therefore it can be calculated directly by inverting Eq. (3.46), to give,

$$E_O(\xi,\eta) = \Im^{-1}\left\{\frac{\Im(E_O(x,y))}{\Im(g(\xi,\eta,x,y))}\right\} \tag{3.50}$$

The advantage of phase shifting Digital Holography is that it produces a reconstructed image of the object without the presence of either the zero order term or the conjugate image. The price for this achievement is the higher technical effort required; phase shifted interferograms have to be generated, thereby restricting the method to slowly varying phenomena with constant phase during the recording cycle.

Phase shifting Digital Holography is illustrated by a holographic image of a nut, shown in Fig. 3.15. This example demonstrates the improvement compared to conventional Digital Holography, as shown in Fig. 3.12.

3.4 Recording of Digital Holograms

3.4.1 Image Sensors

It was the invention of the Charge-Coupled Device (CCD) at Bell Labs, and the dramatic increase in computer storage and processing power which led to the advent of digital holography. More recently, the Complementary Metal Oxide Semiconductor (CMOS) has also become popular for image sensing applications

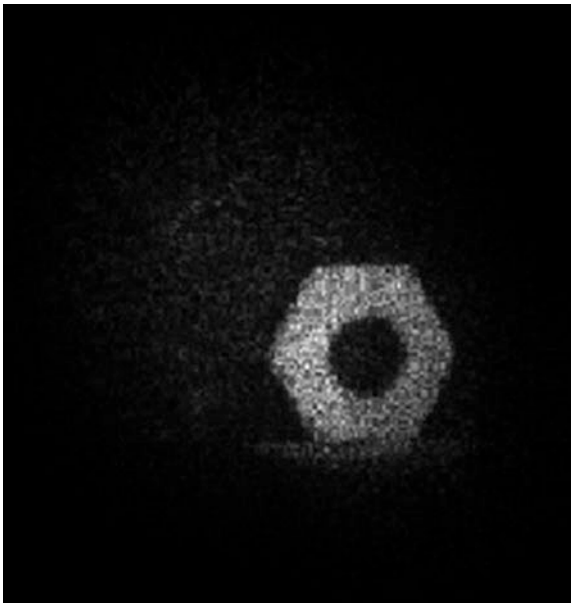

Fig. 3.15 Phase shifting Digital Holography, example (courtesy of S. Seebacher)

and is gradually replacing the CCD in digital still and video cameras. Electronic sensors like CCD or CMOS are composed of arrays of individual light sensitive elements (pixels) which convert incident photons into an induced charge, proportional to the incident intensity that can be stored or transferred through the device. The arrays are sensitive to the spatial variance of the incident light, and are therefore widely used in image recording. Both CCD and CMOS arrays are used in DH. CCDs are generally available as line scanning devices, consisting of a single line of light detectors, and as area scanning devices, consisting of a rectangular 2D matrix of detectors; CMOS are commonly available as area devices. For Digital Holography only the latter architecture is of interest.

To illustrate the concepts of electronic sensors we will base our discussion around the CCD, but the principles of CMOS are broadly similar. Imaging using a CCD sensor is performed in a three-step process [26], involving,

1. Light exposure (the incident light on each pixel is converted into charges by the internal photo effect).
2. Charge transfer (the induced charge packets are moved through the semiconductor (silicon) substrate to memory/storage cells), and,
3. Charge to voltage conversion and output amplification (the capacitor matrix of the memory cells converts the transferred charge to a voltage; an amplifier adapts the voltage to the output requirements).

Three basic architectures are common in CCD sensors *viz.* interline transfer, frame transfer and full-frame transfer configurations respectively.

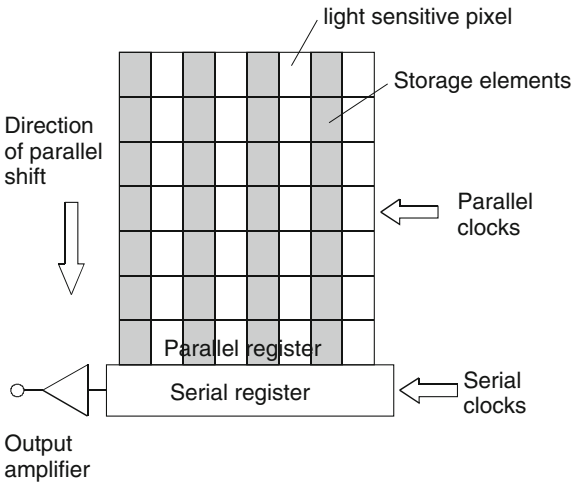

Fig. 3.16 Interline-transfer architecture

Interline (IL) transfer devices consist of rows of light-sensitive detector elements interleaved with rows of non-sensitive or light shielded storage elements, see Fig. 3.16. The charge packets which are generated in the light sensitive pixels are shifted into the adjacent storage area by a parallel clock; and are then shifted line-by-line into a serial register. The serial register transfers the charge packages to an amplified charge-to-voltage converter to form the output signal. The major disadvantage of interline transfer CCDs is their complexity, which results from separating the photo-detecting and storage (readout) functions.

Frame-transfer (FT) CCDs also have different areas for light conversion and for storage but are arranged into two area arrays rather than lines: a light sensitive capture area and a shielded storage area, see Fig. 3.17. The idea is to rapidly shift a captured scene from the photosensitive array to the storage array. The readout from the storage register is performed similarly to the readout process of interline transfer devices.

Full-Frame (FF) sensors have the simplest architecture, see Fig. 3.18. In contrast to IL and FT devices there is no separate storage area. The entire sensor area is light sensitive. The photons are converted into charge packets at each pixel and the resulting rows of image information are then shifted in parallel to the serial register, which subsequently shifts the row of information to the output as a serial stream of data. The process repeats until all rows are transferred off-chip. Since the parallel register is used for both image detection and readout, a mechanical shutter is needed to preserve scene integrity. Full-frame sensors have highest resolution and the production costs are comparably inexpensive.

In principle all three types of sensor are suitable for Digital Holography. Full frame type sensors have the advantage that the exposure time can be adjusted according to the demands of a specific application. Even exposure times in the range of seconds are possible. However, the mechanical shutter limits the number of holograms, which can be recorded per second (frame rate). In addition the shutter

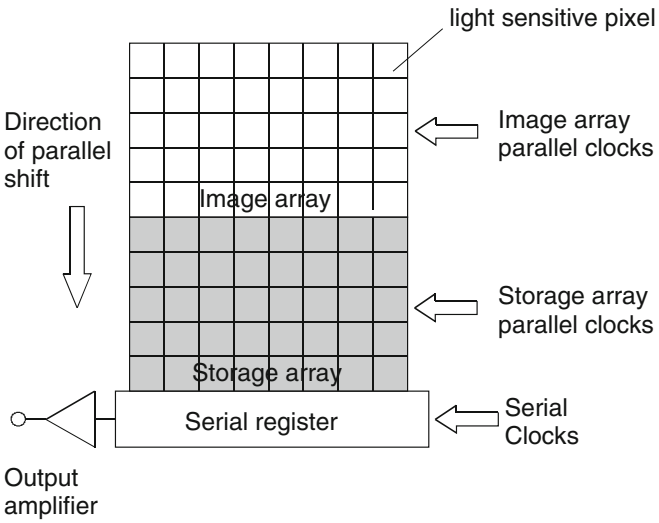

Fig. 3.17 Frame-transfer architecture

Fig. 3.18 Full-frame architecture

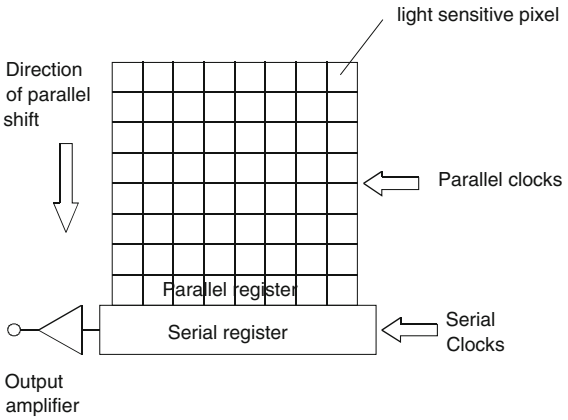

may cause mechanical vibrations to the set-up, which deteriorate the hologram quality. An advantage of interline transfer type sensors is that they are equipped with an electronic shutter, allowing higher frame rates. The best suited camera type depends therefore on the specific holographic application.

In contrast to CCDs each light sensitive pixel of a CMOS sensor is equipped with its own amplifier; i.e. the charge-to-voltage conversion is carried out at pixel level. Each pixel can be read out individually. State-of-the-art CMOS sensors have pixel pitches as small as 1.12 μm (see Table 3.1), which makes them an important alternative for digital holographic applications.

Table 3.1 CCD and CMOS cameras suitable for Digital Holography

Camera	Chip type	Number of pixels	Pixel size (μm^2)	Frames per second	Dynamic range	θ_{max} for λ = 532 nm
Roper Sci. MegaPlus 1.4i	CCD	1,317 × 1,035	6.8 × 6.8	6.9	8 bit	2.2°
GT3300	CCD	3,296 × 2,472	5.5 × 5.5		8 /14 bit	2.8°
Duncan DT1100	CCD	1,392 × 1,040	4.65 × 4.65	12	8 /10 bit	3.3°
DMK 72BUC02	CMOS	1,280 × 960	2.2 × 2.2	15	8 bit	6.9°
Sony CMX081PQ[a]	CMOS	No data	1.12 × 1.12	15	No data	13.6°

[a] For mobile phones

3.4.2 Spatial Frequency Requirements

The CCD or CMOS sensor records the interference pattern resulting from superposition of the reference wave with the waves scattered from the different object points. In order to reduce averaging effects over the area of a pixel, the maximum spatial frequency of the hologram should be smaller than the resolution limit imposed by the sensor. The maximum spatial frequency that can be resolved is determined by the maximum angle θ_{max} between the reference wave and the waves scattered from the different object points according to Eq. (2.30), and given by,

$$f_{max} = \frac{2}{\lambda} \sin \frac{\theta_{max}}{2} \tag{3.51}$$

Photographic emulsions used in classical optical holography have resolutions up to 5,000 line pairs per millimetre (lp/mm). Using these materials, holograms with beam angles of up to 180° can be recorded. However, typical pixel dimensions of CCD/CMOS sensors are around $\Delta x \approx 5$ µm. Consequently, the corresponding maximum resolvable spatial frequency is given by

$$f_{max} = \frac{1}{2\Delta x} \tag{3.52}$$

and is therefore in the range of 100 lp/mm for 5 µm pixels. Combining Eqs. (3.51) and (3.52) leads to a maximum angle, given by

$$\theta_{max} = 2 \arcsin\left(\frac{\lambda}{4\Delta x}\right) \approx \frac{\lambda}{2\Delta x} \tag{3.53}$$

where the approximation is valid for small angles. For a recording wavelength of 532 nm and 5 μm pixels, the maximum recordable angle is about 3.0°. The pixel size therefore limits the maximum angle between the reference and object wave.

3.4.3 Cameras for Digital Hologram Recording

The principle parameters of some selected CCD and CMOS cameras suitable for Digital Holography are listed in Table 3.1.

The sensitivity of CCD or CMOS cameras is typically in the range of 10^{-4} to 10^{-3} J/m^2, which is higher than the sensitivity of photographic emulsions used for classical holography. The spectral response of silicon-based sensors covers the range from approximately 400–1,000 nm. Many commercial cameras are equipped with spectral filters to restrict the sensitivity to the visible spectrum.

In conventional holography with photographic plates the intensity ratio between reference and object wave is normally set to be in the range of 5:1–10:1 in order to avoid nonlinear effects due to the recording medium. However, the maximum contrast in an interference pattern is achieved if the intensity ratio between the two waves is 1:1. Electronic sensors have a much better linearity in the exposure curve than photographic emulsions and consequently, a unity intensity ratio is normally aimed for. As in classical holography the total light energy impinging on the sensor can be controlled by varying the exposure time using a mechanical or the electronic camera shutter.

Currently, CMOS cameras possess the highest resolution (smallest pixel size), see Table 3.1. On the other hand CMOS cameras often have a logarithmic exposure curve. However, this can be tolerated; the advantage of smallest pixel size is more important. The dynamic ranges of CCD- and CMOS-devices is typically 8 bit (256 grey values) or higher. This is comparable with photographic materials and fully sufficient for hologram recording. Even objects with brightness variations exceeding the dynamic range of the recording medium can be stored and reconstructed, because the object information is coded as interference pattern (hologram).

Efficient numerical reconstruction of digital holograms making use of the fast Cooley-Tukey FFT algorithm requires a pixel number, which is a power of 2 (e.g. 1,024 × 1,024). The pixel numbers of some of the cameras listed in Table 3.1 differ from that rule. For a pixel number of e.g. 1,317 × 1,035 (MegaPlus 1.4i) only 1,024 × 1,024 pixels are used for reconstruction. In the case of pixel number slightly lower than a power of 2 it is advisable to add artificial pixels with grey value zero (black) to the recorded hologram until a pixel number of $2^n \times 2^n$ is reached. This *zero padding* does not distort the reconstructed image; it only causes a smoothing or interpolation.

3.4.4 Recording Set-ups

In this section typical arrangements used in Digital Holography are discussed with respect to their spatial frequency limitations. In Fig. 3.19a a plane reference wave propagates perpendicularly to the sensor. The object is located off-axis with respect to the optic axis. This arrangement is very simple, but the space occupied by the object is not used efficiently. The maximum angle between rays emanating from the edge of a cubic object with sides of length L, to the opposite edge of the sensor with sides of length $N\Delta x$ is (distance x shown in Fig. 3.19) is given as

$$\theta_{\max} \approx \frac{x}{d_{\min}} = \frac{\sqrt{\frac{5}{4}}(L + N\Delta x)}{d_{\min}} \tag{3.54}$$

The corresponding minimum object distance d_{min} is calculated by equating this expression with the approximation for $\theta_{\max}$ in Eq. (3.53), and thus,

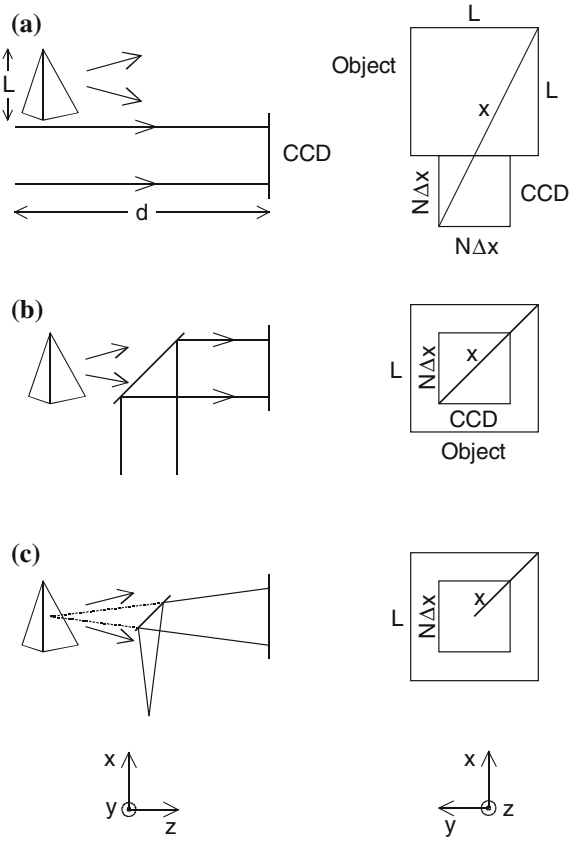

Fig. 3.19 Recording set-ups. *Left* side view; *Right* top view as seen from sensor

$$d_{\min} = \sqrt{\frac{5}{4}}\frac{2\Delta x}{\lambda}(L + N\Delta x) = \sqrt{5}\frac{\Delta x}{\lambda}(L + N\Delta x) \tag{3.55}$$

In Fig. 3.19b the plane reference wave is coupled into the set-up via a beam splitter. This allows positioning the object symmetrically, i.e. objects with larger dimensions can be recorded at a given distance d. The minimum object distance is:

$$d_{\min} \approx \frac{x}{\theta_{\max}} = \sqrt{2}\frac{\Delta x}{\lambda}(L + N\Delta x) \tag{3.56}$$

However, the DC term is in the centre of the reconstructed image and has to be suppressed by the procedures described in Sect. 3.3.1.

Figure 3.19c shows an arrangement for lensless Fourier holography. The spherical reference wave is coupled into the set-up via a beam splitter in order to have the source point in the object plane. The minimum object distance is:

$$d_{\min} = \sqrt{2}\frac{\Delta x}{\lambda}L \tag{3.57}$$

In the lensless Fourier arrangement the shortest object distance can be chosen.

For all the arrangements shown, the maximum spatial frequency has to be adapted very carefully to the resolution of the sensor. If too high a spatial frequency occurs, the contrast of the entire hologram decreases or, in the extreme case, it vanishes totally. In practice, suitably placed apertures, which restrict the lateral propagation help to ensure that the spatial frequency requirements are met.

To record objects with dimensions larger than a few centimetres on a typical sensor, the recording distance d needs to be increased up to several meters. This may not be feasible in practice and recording arrangements are developed to maintain object angles within a resolvable spatial frequency spectrum [180, 203]. A typical example is shown in Fig. 3.20. A diverging lens is placed between the

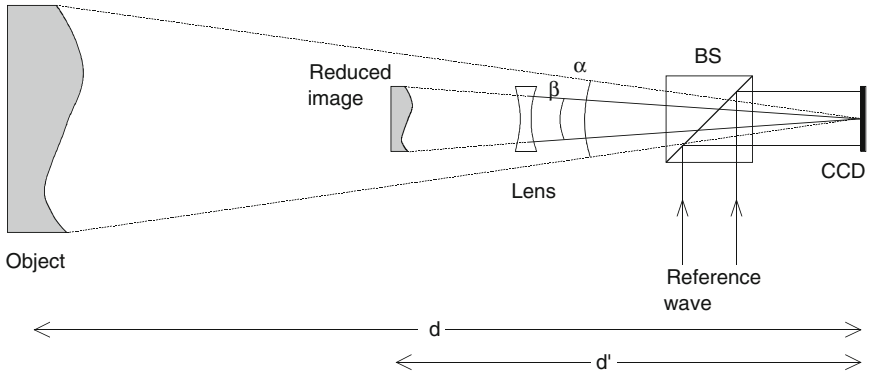

Fig. 3.20 Recording geometry for large objects

object and the target generates a de-magnified virtual image of the object at a distance d'. The wave field emerging from this virtual image is superimposed with the reference wave and the resulting hologram is recorded. The maximum spatial frequency is lower than that of a hologram recorded without object reduction.

3.4.5 Stability Requirements

A stable optical set-up is necessary for digital as well as for conventional holography. Any change in the optical path difference between the interfering beams will result in a movement of the fringes and reduced contrast in the hologram. In practice, the path variation should not exceed 1/4 to 1/10 of a wavelength during hologram exposure. For holography using a continuous wave laser it is essential to mount the optical arrangement on a vibration isolated table. For field holography, a short duration, of the order of a few nanoseconds, pulsed laser is a better option. In contrast to classical holography disturbances due to vibrations are visible in DH even in the recording process: the hologram visible on the monitor of the recording system has a low modulation or the contrast vanishes totally. This is an easy way to monitor the stability of the set-up against vibrations.

3.4.6 Light Sources

The coherence length L_c of the light source used for off-axis holography has to be longer than the optical path difference (OPD) between the reference and object wave paths (measured from the beam splitter to the recording medium) for recording of holograms. If L_c is too short the interference pattern between reference- and object wave vanishes. In practice for most applications the use of a laser is mandatory.

Some commonly used continuous (cw) lasers for Digital Holography and their typical specifications are summarized in Table 3.2. The most common lasers now

Table 3.2 Selected cw lasers for Digital Holography

Laser	Wavelength (nm)	Output power	Coherence length (m)
He–Ne-laser (multi-mode)	632.8	1–50 mW	0.2
Argon-ion laser (single mode)	488/514.5	Up to several W	Up to 100
Frequency doubled Nd:YAG-laser	532	Up to several W	Several 10's
Stabilized diode laser	Various	5–100 mW	Up to 100

used in DH are the frequency-double diode pumped solid state laser (FD-DPSS) and single mode diode lasers.

The FD-DPSS is usually, but not exclusively, based on a doped-insulator crystal such as Nd-YAG; its fundamental wavelength is 1,064 nm producing a frequency-doubled output of 532 nm (the green part of the visible spectrum) over coherence lengths of several tens of meters. It is available either in continuous wave mode (cw), with output powers up to several watts, or in pulsed mode with hundreds of millijoules output over a few nanoseconds duration and at pulse repetition rates of up to 50 Hz. Lower energy (tens of microjoules) models are available with repetition rates up to kilohertz. Flashlamp (rather than diode) pumping can produce energies of several joules. They are rapidly replacing gas and ruby lasers as the preferred option for classical and digital holography.

For field applications out with controlled laboratory conditions, or if moving objects have to be recorded, a pulsed laser is necessary. Formerly ruby lasers were commonly used. Now pulsed Nd:YAG-lasers have better characteristics with respect to compactness, pulse stability and repetition rate.

Diode lasers are also now commonly for continuous wave applications. Single mode operation can be achieved by stabilization electronics. Stabilized diode lasers have long coherence lengths and sufficient output power. However, the wavelength is not fixed by atomic transitions as for the lasers discussed above. That means it is necessary to monitor its wavelength during operation. In addition the wavelength depends on the temperature, typical drift is of the order of 0.2 nm/°C. On the other hand their wavelengths are tuneable over the order of several nanometers. Tuneable diode lasers are used for two-wavelength contouring for example.

Another interesting type of light source for DH is the superluminescent diode (SLED or SLD). Such diodes combine the high output power of laser diodes with the low temporal coherence of conventional LED's. These devices are the ideal choice, if low coherent noise but high brightness is necessary.

In the early days of holography, both classical and digital, gas lasers such as Helium-Neon (HeNe) and argon ion were almost exclusively used for continuous wave holography and ruby lasers for pulsed holography. The Helium-Neon (He–Ne) laser is able to operate at several different wavelengths, but mostly commonly the red 632.8 nm line is used. He–Ne lasers are moderately inexpensive, the technology is mature and still found in many laboratories and schools for educational uses of holography. When DH was in its infancy, and only sensors with pixel sizes of about 10 μm were available, the relatively long wavelength was advantageous, because it allowed larger angles between the interfering waves (see Sect. 3.4.2). Unstabilized He–Ne lasers oscillate on several longitudinal modes. The coherence length of such lasers is therefore not determined by the width of a single mode, but by the width of the entire gain profile and is in the order of 20 cm.

The spatial coherence of the laser is also crucial in holography. Only with an object illumination of sufficient spatial coherence it is possible to generate a scattered light field with defined complex amplitude in the far field domain of the object. The lasers discussed above usually oscillate in a single transverse mode (TEM_{00}) and have a Gaussian profile.

For some special applications in microscopy, particle sizing or in shearing interferometry the requirements on temporal coherence are lower than for off-axis holography. In this case light emitting diodes (LED's) can often be used. LED's have a spectral width of about 10 nm or, equivalently, a coherence length in the range of 50 µm. This is sufficient if the OPD is sufficiently low. In Chap. 7 we present some computational methods which enable sensing of low coherence wave fields as well. This enables applications very similar to those applicable for DH, such as numerical refocusing for example, but using low coherent light provided by an LED.